HHS Public Access

Author manuscript

Biochem J. Author manuscript; available in PMC 2016 June 15.

Published in final edited form as:

Biochem J. 2015 December 15; 472(3): 339–352. doi:10.1042/BJ20150410.

Phosphoregulation of the *C. elegans* cadherin–catenin complex

Sandhya Callaci[*], **Kylee Morrison**[*], **Xiangqiang Shao**[†], **Amber L. Schuh**[*], **Yueju Wang**[‡], **John R. Yates III**[‡], **Jeff Hardin**[†], and **Anjon Audhya**[*,1]

[*]Department of Biomolecular Chemistry, University of Wisconsin-Madison School of Medicine and Public Health, Madison, WI 53706, U.S.A.

[†]Department of Zoology and Program in Genetics, University of Wisconsin-Madison, Madison, WI 53706, U.S.A.

[‡]Department of Cell Biology, The Scripps Research Institute, La Jolla, CA 92037, U.S.A.

Abstract

Adherens junctions play key roles in mediating cell–cell contacts during tissue development. In *Caenorhabditis elegans* embryos, the cadherin–catenin complex (CCC), composed of the classical cadherin HMR-1 and members of three catenin families, HMP-1, HMP-2 and JAC-1, is necessary for normal blastomere adhesion, gastrulation, ventral enclosure of the epidermis and embryo elongation. Disruption of CCC assembly or function results in embryonic lethality. Previous work suggests that components of the CCC are subject to phosphorylation. However, the identity of phosphorylated residues in CCC components and their contributions to CCC stability and function in a living organism remain speculative. Using mass spectrometry, we systematically identify phosphorylated residues in the essential CCC subunits HMR-1, HMP-1 and HMP-2 *in vivo*. We demonstrate that HMR-1/cadherin phosphorylation occurs on three sites within its β-catenin binding domain that each contributes to CCC assembly on lipid bilayers. In contrast, phosphorylation of HMP-2/β-catenin inhibits its association with HMR-1/cadherin *in vitro*, suggesting a role in CCC disassembly. Although HMP-1/α-catenin is also phosphorylated *in vivo*, phosphomimetic mutations do not affect its ability to associate with other CCC components or interact with actin *in vitro*. Collectively, our findings support a model in which distinct phosphorylation events contribute to rapid CCC assembly and disassembly, both of which are essential for morphogenetic rearrangements during development.

Keywords

conformational change; recombinant protein expression; small-angle X-ray scattering (SAXS)

[1]To whom correspondence should be addressed (audhya@wisc.edu).

AUTHOR CONTRIBUTION

Sandhya Callaci, Kylee Morrison, Xiangqiang Shao, Amber Schuh and Anjon Audhya conceived and designed experiments. Sandhya Callaci, Kylee Morrison, Xiangqiang Shao, Amber Schuh, Yueju Wang, John Yates III, Jeff Hardin and Anjon Audhya performed experiments and analysed data. All authors discussed the results, and Anjon Audhya wrote the final version of the manuscript.

INTRODUCTION

Intercellular junctions, including adherens junctions, tight junctions and gap junctions, enable cell adhesion and communication between juxtaposed endothelial or epithelial cells within tissues, which is essential for normal development in all metazoan organisms [1–3]. In the cardiovascular system, for example, adherens junctions play essential roles in paracellular permeability and new blood vessel growth [4]. The major components of adherens junctions include transmembrane cadherins and associated cytoplasmic catenins. Based on amino acid sequence comparisons and structural features, more than 30 members of the cadherin family have been identified in mammals [5]. However, only one isoform is expressed in the vascular endothelium: the classical cadherin, VE-cadherin. Like other classical cadherins, VE-cadherin exhibits (1) an extracellular amino-terminus that can multimerize and interact in *trans* with other cadherin molecules expressed on adjacent cells, (2) a single-pass transmembrane domain and (3) a cytoplasmic carboxyl-terminus that binds to β-catenin and p120 catenin [6,7]. In turn, β-catenin recruits α-catenin, which functions to control binding to and bundling of actin filaments that strengthen adhesion [8]. Kinases, phosphatases and ubiquitin ligases also regulate the function of cadherin and catenin complexes (CCCs) to modulate stability of adherens junctions [9,10].

Just as important as the formation of adherens junctions is their disassembly, which is critical for tissue remodelling. The mechanisms that underlie removal of CCCs from cell–cell junctions remain unclear. However, evidence suggests important roles for post-translational modification of cadherins and catenins during this process [11,12]. Nearly two decades ago, the anchorage of cadherins to the cytoskeleton was shown to be regulated by tyrosine phosphorylation [13–15]. In epithelial cells, activation of receptor tyrosine kinases in response to growth factor signalling results in phosphorylation and ubiquitinylation of E-cadherin, inducing its endocytosis and transport to the lysosome for degradation [10]. Equivalent events probably govern the down-regulation of other cadherin isoforms. Supporting this idea, previous studies have shown that VE-cadherin is subject to clathrin-mediated endocytosis, and inhibition of endosomal/lysosomal-mediated degradation stabilizes ubiquitinylated VE-cadherin [16,17]. Together, these data suggest that the endocytic pathway regulates the stability of adherens junctions, both in endothelial and epithelial cells, in a manner that is dependent on post-translational modifications of CCCs.

The nematode *Caenorhabditis elegans* expresses only a single classical cadherin in all epithelia, HMR-1, which binds directly to the β-catenin HMP-2 and the p120 catenin JAC-1 at cell–cell junctions [18]. HMP-2 further associates with the α-catenin HMP-1, forming a CCC that regulates cell adhesion during early embryonic development, including gastrulation, ventral enclosure and embryonic elongation. Loss of HMR-1, HMP-2 or HMP-1 leads to dramatic defects in morphogenesis and embryonic lethality. The relative simplicity of this junctional complex affords unique opportunities to dissect key regulatory events that control CCC assembly and disassembly. Indeed, previous work has identified the PAR/aPKC complex and LET-413/Scribble as important regulators of CCC establishment and organization [19,20]. Additionally, numerous conserved, functional partners for CCCs have been identified in *C. elegans*, including ZOO-1/ZO-1, SRGP-1/srGAP and UNC-34/Enabled, using a combination of genetic and biochemical approaches [18,21]. However, no

previous studies have examined the state of CCC components extracted directly from living embryos. Here, we purify each CCC component from *C. elegans* embryos and identify a series of phosphorylation sites by mass spectrometry, which contribute to CCC stability and function. Our data strongly suggest that phosphorylation of HMR-1 increases its association with HMP-2, whereas phosphorylation of HMP-2 inhibits binding to HMR-1. In contrast, a phosphomimetic form of HMP-1 interacts normally with HMP-2 and actin *in vitro*. Using SAXS, we further demonstrate that phosphomimetic mutations in HMP-1 do not alter its global fold, suggesting that phosphorylation plays an alternative role in regulating α-catenin function *in vivo*. Collectively, our data highlight the importance of phosphoregulation in controlling CCCs, which probably applies to related junctional complexes found in other organisms, including mammals.

EXPERIMENTAL

Immunoprecipitation and mass spectrometry

Adult hermaphrodites were grown in liquid culture and embryos were isolated as described previously [22]. Immunoprecipitations from clarified embryo extracts were conducted in lysis buffer (50 mM Hepes, 1 mM EDTA, 1 mM $MgCl_2$, 100 mM KCl and 10% glycerol) supplemented with 1% Triton X-100 and protease inhibitors using antibodies that were coupled covalently to protein A resin. For mass spectrometry analysis, purified proteins were eluted from resin using 100 mM glycine (pH 2.6), TCA precipitated and processed for multidimensional protein identification technology (MudPIT) analysis [22,23]. Spectra were searched using the ProLuCID [24] algorithm against the *C. elegans* database (Wormbase). For phosphosite mapping, extracts were supplemented with phosphatase inhibitors (sodium orthovanadate, β-glycerophosphate and sodium pyrophosphate) prior to immunoprecipitation and throughout the purification process [25]. Spectra were annotated by hand, and a probability-based score (Ascore) was used to determine phosphorylation site localization [26].

Protein purification and gel filtration studies

Recombinant protein expression was performed using BL21-T1R (DE3) *E. coli*. For purification of HMP-1 and HMP-2, cDNAs were cloned into pGEX6P-1, which encodes a cleavable, amino-terminal GST tag. For co-purification studies, GST-HMP-2 was co-expressed with His-SUMO tagged HMP-1. Affinity tags were removed using Prescission protease or SUMO protease, respectively, prior to further analysis of complexes formed. Protein purifications were conducted using glutathione agarose beads (for all GST fusion proteins) or nickel affinity resin (for purification of polyhistidine-tagged forms of the HMR-1 cytoplasmic domain, which was cloned into the pRSETA bacterial expression construct). Following affinity purification, all proteins (1 ml) were applied to either a Superose 6 or S200 size-exclusion column (GE Healthcare) equilibrated in 50 mM Hepes (pH 7.6), 1 mM DTT, 100 mM KCl. 1 ml fractions were collected during each size-exclusion chromatography (SEC) experiment and analysed by SDS/PAGE analysis. Densitometry of bands was used to calculate peak elution volumes, which were compared with those of characterized standards with known Stokes radii. Samples for SAXS were dialysed overnight into SAXS buffer (50 mM Tris (pH 8.0), 10 mM DTT and 100 mM

NaCl). Light-scattering data were collected using a Wyatt mini-DAWN TREOS three-angle light-scattering detector coupled to a high-resolution size-exclusion column. Data were collected at a flow rate of 0.5 ml/min and analysed with the ASTRA software to determine molecular masses of proteins [27].

To generate a *C. elegans* embryo extract for gel filtration analysis, adult hermaphrodites were first grown in liquid culture and embryos were isolated as described previously [22]. Embryos were mechanically disrupted in liquid nitrogen using a mortar and pestle, resuspended in lysis buffer (50 mM HEPES (pH 7.6), 1 mM EGTA, 1 mM $MgCl_2$, 100 mM KCl, 10% glycerol and 2 mM PMSF), sonicated and subjected to centrifugation at 50,000 RPM. The supernatant was loaded on to a Superose 6 gel filtration column and 1 ml fractions were collected for SDS/PAGE and immunoblot analysis. Since detergent was omitted during all steps of extract preparation, only cytosolic proteins were able to be studied using this approach.

SAXS data collection

SAXS data were obtained at Sector 12 of the Advanced Photon Source at Argonne National Laboratory. Data for buffer and protein were collected at 25°C. To account for excluded volume of the protein, buffer was subtracted. Guinier analysis was conducted to determine the Rg values through the use of the Primus software (ATSAS) [28,29]. Processing of SAXS data was performed with Gnom software (ATSAS) [28]. The discrepancy between our Rg determination for wild-type HMP-1 and data published previously [21] is a result of the prior study mistakenly using a truncated form of HMP-1 (personal communication from William Weis, W. James Nelson and Adam Kwiatkowski).

Production of liposomes and co-flotation assays

Liposomes (78% phosphatidylcholine, 18% phosphatidylethanolamine (PE), 2% 1,2-dioleoyl-sn-glycero-3-[(*N*-(5-amino-1-carboxypentyl) iminodiacetic acid) succinyl] nickel salt (DOGS-NTA-Ni) and 2% rhodamine-labelled PE) were prepared by extrusion through polycarbonate filters with a pore size of 100 nm (Avanti Polar Lipids). For co-flotation assays, preformed liposomes (1 mM) were incubated with all proteins used in the assay simultaneously (200 nM HMP-1, 200 nM HMP-2 and/or 400 nM HMR-1 cytoplasmic domain) in buffer (50 mM Hepes (pH 7.6), 100 mm KCl and 1 mM DTT) prior to mixing with Accudenz density medium. Mixtures were overlaid with decreasing concentrations of Accudenz (0–40%) and centrifuged for 2 h at 280,000 × ***g***. During this period, liposomes and associated proteins floated to the buffer/Accudenz interface and were harvested by hand. Recovery of liposomes was normalized based on the fluorescence intensity of the sample, and equivalent fractions were separated by SDS/PAGE and subjected to silver-stain analysis to determine the relative amount of protein that bound [30]. To study the role of HMR-1 phosphorylation on CCC assembly on liposomes, the purified HMR-1 cytoplasmic domain (40 μM) was incubated with casein kinase I (CK1) (1000 units; New England Biosciences), the vendor supplied kinase buffer and ATP (200 μM) for 30 min at room temperature (in the absence of the catenins). Following the kinase reaction, phosphorylated HMR-1 was subjected to ion exchange chromatography followed by SEC to remove any residual kinase.

The purified, phosphorylated HMR-1 was then used in co-flotation assays as described earlier.

Actin pelleting assays

Rabbit skeletal muscle G-actin (Cytoskeleton) was polymerized for 1 h at 25°C to generate F-actin in polymerization buffer (5 mM Tris, pH 8.0, 0.2 mM $CaCl_2$, 0.5 mM DTT, 50 mM KCl, 2 mM $MgCl_2$, 1.2 mM ATP). HMP-1 isoforms (2 μM) were incubated with 0, 2 or 5 μM F-actin in reaction buffer (50 mM Hepes, pH 7.6, 0.1 M KCl, 10% glycerol, 0.5 mM DTT, 0.2 mM ATP, 0.2 mM $CaCl_2$) for 30 min at 25°C. Samples were centrifuged at 100,000 × ***g*** for 20 min, which is sufficient to pellet all actin and proteins bound to actin. Supernatant and pellet samples were prepared at the same dilution in Laemmli sample buffer and separated on a SDS/PAGE (12% gel), which was subsequently stained using Coomassie. Band intensity was measured and quantified using Photoshop, and further analysis was carried out in Microsoft Excel.

Antibody production and purification

C. elegans HMP-1, HMP-2 and HMR-1 antibodies were raised in rabbits by immunization (Covance) with GST-tagged HMP-1 (full-length), HMP-2 (full-length) and HMR-1 (cytoplasmic domain, residues 1108–1123) produced in *E. coli*. Antibodies were subsequently affinity purified from serum by binding to columns harbouring untagged forms of the different antigens. Antibody specificity was verified by immunofluorescence, using control embryos or embryos individually depleted of endogenous HMP-1, HMP-2 or HMR-1. In each case, loss of the endogenous protein resulted in the absence of antibody staining at cell junctions.

Transgenic strains and fluorescence microscopy

A Nikon Eclipse E600 microscope equipped with a Yokogawa CSU10 spinning disk scanhead and a Hamamatsu ORCA-ER CCD camera was used to image transgenic strains. Animals expressing HMP-2::GFP and HMP-2^{4E}::GFP were generated by injecting plasmids expressing these fusions into wild-type worms and crossing them into *hmp-2* (*zu364*) heterozygotes.

RESULTS

Native HMR-1 is phosphorylated and forms a stable complex with multiple catenin isoforms

To determine the molecular composition of HMR-1 complexes in *C. elegans* embryos, we took advantage of affinity-purified antibodies directed against the protein, which we developed and characterized previously [31], to isolate endogenous HMR-1 from detergent-solubilized extracts (Figure 1A). In three separate experiments, we consistently recovered a large number of peptides corresponding to HMR-1 (greater than 50%sequence coverage) subsequent to MudPIT analysis (Table 1). Additionally, after subtracting contaminants that are common to other unrelated purifications, we identified members of each catenin family, including HMP-1 (α-catenin), HMP-2 (β-catenin) and JAC-1 (p120 catenin), as well as peptides corresponding to the *C. elegans* homologue of afadin (AFD-1), a previously

identified actin filament-binding protein that is enriched at adherens junctions (Table 1) [32]. The interactions between HMR-1, HMP-1 and HMP-2 were further confirmed by immunoblot analysis (Figure 1B). These data demonstrate our ability to recover intact CCCs by immunoprecipitation from embryo extracts.

Previous work indicates that serine/threonine phosphorylation of cadherin isoforms is required for their stable association with β-catenins. Both directed and unbiased mutagenesis approaches have been used to identify putative sites of phosphorylation within the carboxyl-terminus of E-cadherin [33,34], but efforts to directly determine the residues that are modified *in vivo* have not been described. We therefore purified HMR-1 from *C. elegans* embryo extracts in the presence of phosphatase inhibitors and determined phosphorylation sites by mass spectrometry (Figures 1C and 1D). This approach reproducibly revealed three phosphorylation sites in HMR-1 (each was observed in three independent phosphoproteomic analyses), all within its conserved β-catenin binding site (S1212, T1215 and S1218). Strikingly, serines 1212 and 1218 in HMR-1 correspond to serines 840 and 847 in human αE-cadherin, which were identified as putative phosphorylation sites based on *in silico* predictions and *in vitro* assays [33]. However, our results suggest that serine 844 in E-cadherin, which corresponds to T1215 in HMR-1, is also subject to phosphorylation *in vivo*, contrasting with prior bioinformatics results that suggested serine 846 in E-cadherin is endogenously phosphorylated [33]. Together, our findings indicate that native HMR-1 is phosphorylated on three conserved residues, which may play important roles in regulating its ability to associate with HMP-2/β-catenin. Consistent with this idea, a HMR-1 transgene with an alanine substitution at position 1212 (prohibiting phosphorylation at this site) fails to complement loss of endogenous HMR-1 function, with animals arresting during embryonic development. Additionally, a HMR-1 transgene harbouring alanine substitutions at positions 1215 and 1218, while retaining some function, also fails to rescue embryos lacking endogenous HMR-1 to adulthood, with animals exhibiting penetrant larval lethality [35].

HMP-1 and HMP-2 associate with multiple junctional components and are also subject to phosphorylation *in vivo*

Using affinity-purified antibodies directed against HMP-1 and HMP-2 [31], we also performed a series of immunoprecipitations followed by MudPIT analysis to define the binding partners of the junctional α- and β-catenins in worms (Table 1; Figure 1A). Common to both purifications were HMP-1, HMP-2, JAC-1, HMR-1 and AFD-1, which were all identified following immunoprecipitation of HMR-1. Additionally, we also identified SRGP-1 and MAGI-1, two previously characterized junctional components that each facilitates cell–cell adhesion during *C. elegans* embryonic morphogenesis, in both purifications (Table 1) [31,32]. These data support the idea that HMP-1, HMP-2 and HMR-1 establish the foundation of an interaction network that enables the formation of adherens junctions.

We further used mass spectrometry to identify phosphorylation sites in native HMP-1 and HMP-2 (Figures 2, 3A and 3B). In total, we reproducibly found that each is phosphorylated on multiple residues *in vivo*. In the case of HMP-1, we consistently observed modification on four serines scattered throughout the protein (312, 509, 649 and 910; all residues were

identified in each of three independent phosphoproteomic analyses), but none were found at characterized interfaces for F-actin or β-catenin binding [18]. In contrast with this distribution, phosphorylation of HMP-2 was concentrated within a small region near its carboxyl-terminus (tyrosines 622 and 624 and serines 619 and 621; all were identified in each of three independent phosphoproteomic analyses). Interestingly, tyrosine 654 in human β-catenin is subject to phosphorylation, which leads to a 6-fold reduction in its affinity for E-cadherin [12]. However, we failed to identify phosphorylation of the homologous tyrosine residue (Y599) in our *in vivo* analysis of HMP-2. Nonetheless, phosphorylation of HMP-2 may similarly affect its association with HMR-1.

To explore this question further, we conducted a series of *in vivo* rescue experiments using either wild-type HMP-2 or a mutant form of HMP-2 harbouring four phosphomimetic (glutamic acid) substitutions at residues 619, 621, 622 and 624 (HMP-2^{4E}). Each was overexpressed as a GFP fusion in mutant animals that were homozygous for the *hmp-2* loss of function allele *zu364* (Figure 3C). In the absence of transgene expression, none of the mutant embryos were viable (n = 101 embryos). Moreover, while the wild-type form of HMP-2 fully complemented the *zu364* allele (24/24 embryos expressing the transgene survived), we observed that a substantial fraction of embryos overexpressing HMP-2^{4E} failed to live (5/36 embryos died). We next compared the distributions of the wild-type protein and HMP-2^{4E}, and we found that they accumulated equivalently at cell–cell junctions (Figures 3D–3F). However, there are several challenges to interpreting these data. Although the *zu364* allele encodes a non-functional form of HMP-2, the protein still localizes to adherens junctions, and may facilitate the recruitment of HMP-2^{4E}. Additionally, the phosphomimetic mutations generated may not fully recapitulate the effect of HMP-2 phosphorylation *in vivo*. An alternative possibility is that phosphorylation of HMR-1 plays a more prominent role in regulating its association with HMP-2, whereas HMP-2 phosphorylation functions to further modulate the interaction *in vivo*. Taken together, our data suggest that mutations that mimic constitutive phosphorylation at residues 619, 621, 622 and 624 impair HMP-2 function, but in a manner that cannot be easily assessed by localization studies in animals.

Recombinant HMP-1 does not self-associate, but HMP-2 forms dimers that are capable of further oligomerization *in vitro*

Previous work using native gels and SEC suggested that HMP-1 fails to homodimerise, in contrast with its mammalian counterparts [21]. To verify these findings, we purified bacterially expressed, full-length HMP-1, subjected it to SEC, coupled to multi-angle light scattering (SEC–MALS), and eluted fractions were analysed by SDS/PAGE (Figures 4A–4C). These data demonstrated that HMP-1 exhibits an average Stokes radius of approximately 42 Å (1 Å=0.1 nm) and a molecular mass of 112.8 kDa (±0.4 %), very close to that predicted by its amino acid composition (104 kDa). In contrast, recombinant, full-length HMP-2 was found to exist in two distinct populations following gel filtration chromatography and SDS/PAGE analysis, with average Stokes radii of 49 Å and 101 Å (Figure 5A; highlighted in green and orange, respectively). We isolated each pool of HMP-2, further purified and concentrated them individually using anion exchange chromatography, and took advantage of SEC–MALS to show that the 49 Å population

exhibited a molecular mass of 147.1 kDa (± 1.8 %), similar to that of a dimer (149 kDa, as predicted by amino acid composition), whereas the 101 Å population exhibited a 10-fold larger mass in the megadalton range (Figures 5B–5E). These data highlight the ability of recombinant HMP-2 to oligomerize when purified in the absence of other CCC components *in vitro*.

To compare the hydrodynamic properties of recombinant HMP-1 and HMP-2 with their endogenous counterparts, we subjected *C. elegans* embryos to mechanical homogenization and high-speed centrifugation to generate an extract that was analysed by SEC. Immunoblot analysis of the eluted fractions indicated that HMP-1 and HMP-2 co-migrated through the column, exhibiting an average Stokes radius of 52 Å (Figure 5F). These data suggest that HMP-1 and HMP-2 are largely found in a common protein complex *in vivo*. In parallel with these studies, we also co-expressed HMP-1 and GST-tagged HMP-2 in bacteria, and purified the complex using glutathione agarose beads. Following elution, removal of the GST tag using PreScission protease, and SEC, we found that both HMP-1 and HMP-2 co-eluted as a complex with an average Stokes radius of 53 Å, similar to that observed for endogenous HMP-1 and HMP-2 (Figure 5G). Furthermore, under these conditions, we failed to isolate the large, homo-oligomeric HMP-2 population, suggesting that in the presence of HMP-1, HMP-2 does not self-associate *in vitro*. Together, these data support the idea that HMP-1 and HMP-2 form a stable complex *in vivo*, which can bind to HMR-1 at adherens junctions.

Reconstitution of CCCs on liposomes reveals that phosphorylation of HMR-1 facilitates its association with HMP-1/HMP-2 complexes

To study the impact of phosphorylation on CCC formation in a more physiologically relevant setting, we developed a method to reconstitute the complex on model lipid bilayers. To do so, we fused a polyhistidine tag to the cytoplasmic carboxyl-terminus of HMR-1 (amino acids 1108–1223), and incubated the purified protein together with an equimolar concentration of the untagged HMP-1/HMP-2 complex and liposomes harbouring the metalion-chelating (polyhistidine-binding) lipid, DOGS-NTA-Ni. The protein and membrane mixture was placed under a gradient of Accudenz and subjected to high-speed centrifugation. During this time, vesicles and associated proteins floated to the top of the gradient and were recovered by hand. Samples were normalized based on the concentration of vesicles, and co-floated proteins were separated by SDS/PAGE. Under these conditions, we found that unmodified HMR-1 facilitated the association of HMP-1 and HMP-2 with liposomes (Figures 6A and 6B). In contrast, we were only able to recover negligible amounts of HMP-1 and HMP-2 in the absence of HMR-1, indicating that neither protein associates with the bilayer non-specifically nor do proteins become trapped within liposomes during the course of the experiment. These data highlight a new approach to studying CCC assembly on model lipid bilayers.

Previous work suggested that *in vitro* phosphorylation of HMR-1$^{1108–1223}$ using CK1 promotes its association with the HMP-1/HMP-2 complex in solution [21]. We confirmed these data using our membrane-based reconstitution system and demonstrated a 6-fold enhancement in HMP-1/HMP-2 recovery in the presence of CK1-phosphorylated

HMR-1$^{1108–1223}$ as compared with unphosphorylated HMR-1 (Figures 6A and 6B). To determine the contributions of specific HMR-1 phosphorylation sites we identified *in vivo* to the recruitment of HMP-1 and HMP-2 to membranes, we generated a series of phosphomimetic isoforms of polyhistidine-tagged HMR-1$^{1108–1223}$. In particular, we focused on the role of serine 1212 phosphorylation (HMR-1^{S1212E}), since previous work suggested that a homologous residue is modified in human E-cadherin. Additionally, we generated forms of HMR-1 harbouring 2 or 3 phosphomimetic substitutions (HMR-1^{T1215E,S1218E} and HMR-1^{S1212E,T1215E,S1218E}). Each isoform of HMR-1$^{1108–1223}$ exhibited a distinct migration rate during SDS/PAGE (phosphomimetic mutations caused more rapid movement), which we also observed when comparing the CK1-phosphorylated and unphosphorylated proteins (Figure 6C). Our findings demonstrated that a single phosphomimetic mutation at residue 1212 resulted in a significant 1.8-fold increase in HMP-1/HMP-2 recovery following co-flotation, while two substitutions at positions 1215 and 1218 enhanced HMP-1/HMP-2 binding by approximately 1.4-fold (Figures 6D and 6E). When all three mutations were present, we found a 2.2-fold elevation in HMP-1/HMP-2 association, suggesting that the phosphorylation of all three sites promotes CCC formation in an additive, but not cooperative, manner (Figures 6D and 6E). These data strongly suggest that each of the three phosphorylation events contributes to the regulation of adherens junction formation.

Phosphorylation of HMP-1 and HMP-2 at endogenous phosphosites identified by mass spectrometry does not affect their association with one another

Although phosphosites identified in endogenous HMP-1 and HMP-2 were not distributed at the interface between the proteins, we investigated the potential impact of phosphomimetic mutations on the co-assembly of the HMP-1/HMP-2 complex. We used phosphomimetic forms of HMP-1 and HMP-2 in which all phosphorylated sites identified *in vivo* were mutated to glutamic acid (HMP-1^{4E} and HMP-2^{4E}). Following co-expression in bacteria, we took advantage of SEC in an attempt to identify any changes in the co-assembly of HMP-1 and HMP-2 in the presence or absence of phosphomimetic mutations. However, we found that no combinations examined affected the degree to which the heterodimers formed, nor did phosphomimetic mutations significantly affect the average Stokes radius of the complex (Table 2). These data suggest that phosphorylation of HMP-1 and HMP-2 at the residues we identified as endogenous phosphosites does not affect their ability to associate with one another.

Phosphorylation of HMP-2 impairs its ability to associate with HMR-1

Previous work demonstrated that HMP-2, but not HMP-1, associates directly with HMR-1 at CCCs [36]. To define a potential role of HMP-2 phosphorylation *in vivo*, we first studied the impact of HMP-2 phosphomimetic mutations on HMR-1 binding using our co-flotation assay. For all experiments, we again used the cytoplasmic region of HMR-1 harbouring a polyhistidine tag, which associates directly with DOGS-NTA-Ni-containing liposomes. In the presence of wild-type HMR-1$^{1108–1223}$ (no phosphomimetic mutations), nearly 2-fold less HMP-1/HMP-2^{4E} co-floated with liposomes as compared with wild-type HMP-1/HMP-2 (Figure 7; relative to the amount of HMP-1/HMP-2 that non-specifically co-floated in the absence of a HMR-1 isoform). These data suggest that phosphorylation of HMP-2

diminishes its ability to associate with HMR-1 on membranes. We further tested the impact of phosphomimetic mutations in HMP-2 on its binding to phosphomimetic HMR-1. Under these conditions, we found a 10-fold reduction in HMP-1/HMP-2^{4E} binding to HMR-1^{3E}, as compared with wild-type HMP-1/HMP-2 binding to HMR-1^{3E} (Figure 7). These data support a model in which phosphorylation of HMP-2 diminishes its affinity for HMR-1. However, based on our localization studies *in vivo*, as well as those performed previously [35], the role of HMP-2 phosphoregulation in controlling its distribution in cells appears to be relatively modest as compared with the role of HMR-1 phosphorylation at adherens junctions.

Phosphomimetic mutations in HMP-1 do not affect its global conformation or its ability to bind actin *in vitro*

Previous data suggested that HMP-1 links the CCC to the underlying actin cytoskeleton [37]. Although the carboxyl-terminus harbours a *bona fide* actin-binding domain, the full-length protein has been suggested to exhibit an autoinhibited conformation, limiting its ability to associate with actin [21]. We therefore sought to determine whether phosphomimetic mutations in HMP-1 affect its conformation. Analysis of HMP-1^{4E} using SEC revealed no difference in its hydrodynamic radius as compared with unmodified HMP-1 (Figure 8A; compare to Figure 4A). We further used SAXS across three different protein concentrations to demonstrate that wild-type full-length HMP-1 exhibits an average radius of gyration of 41.6 Å (Figure 8B and Table 3). Notably, the hydrodynamic radius we determined was nearly equivalent to the radius of gyration, suggesting that HMP-1 is not spherical, but instead more linear in solution, consistent with the presence of multiple coiled-coil domains throughout the protein [38]. Analysis of the phosphomimetic form of HMP-1 (HMP-1^{4E}) revealed a highly similar radius of gyration (42.5 Å, on average between three concentrations of the protein), as compared with the wild-type protein (Figure 8C and Table 3). Additionally, using the SAXS data, we also compared plots of the scattering vector (*s*) as a function of the intensity (*I*) for both forms of HMP-1 and found that they were nearly identical (Figure 8D). These data suggest that phosphorylation of HMP-1 does not result in a global change in its conformation. Instead, it is more likely that local changes in HMP-1 conformation occur upon its post-translational modification. However, there exist a number of caveats associated with this conclusion that bear mentioning. For example, phosphomimetic residues such as glutamic acid exhibit reduced charge as compared with residues that are actually phosphorylated. Thus, the phosphomimetic form of HMP-1 may not induce the same conformational change as direct phosphorylation would. Additionally, the ability of gel filtration analysis and SAXS studies to resolve conformational changes in elongated proteins is relatively limited. With these caveats in mind, we decided to explore the potential functional consequences of HMP-1 phosphorylation.

Although the phosphorylated residues in HMP-1 are not within its actin-binding domain, we sought to determine whether potential local conformational changes resulting from phosphorylation affected actin binding. We therefore conducted a series of actin pelleting assays with HMP-1 and HMP-1^{4E}. At two different concentrations of actin (2 and 5 μM), we reproducibly demonstrated that the phosphomimetic mutations in HMP-1 did not alter its very weak association with actin (Figure 9). These data suggest that serine phosphorylation

ofHMP-1 does not play a role in regulating its ability to link CCCs to the actin cytoskeleton, but instead regulates α-catenin in a distinct manner.

DISCUSSION

Components of the CCC enable cell adhesion in epithelial tissues in diverse organisms, ranging from worms to humans. Dynamic alterations in cell–cell contacts during embryonic morphogenesis necessitate mechanisms to rapidly assemble and disassemble junctional complexes. Although previous work raised the possibility that phosphorylation of CCC subunits modulates the stability of adherens junctions [9,11–14,33,39,40], the sites modified *in vivo* have not been identified in a comprehensive manner. Here, taking advantage of the simple *C. elegans* CCC, we systematically mapped phosphorylation sites within three foundational components of the CCC using mass spectrometry. We further demonstrated the distinct functions of cadherin (HMR-1), α-catenin (HMP-1) and β-catenin (HMP-2) phosphorylation *in vitro*, demonstrating that each event affects CCC function in a distinct manner. While phosphorylation of HMR-1 probably promotes CCC formation, post-translational modification of HMP-2 disrupts CCC assembly. Although the kinases directly responsible for CCC phosphorylation *in vivo* remain unknown, our data suggest they must function at distinct steps and/or in a coordinated manner with specific phosphatases to appropriately control CCC function during development.

Previous work identified a conserved serine/threonine-rich segment within the carboxyl-terminus of vertebrate E-cadherin that is responsible for binding to β-catenin. Mutation of all serine residues in this domain to alanine impairs binding to β-catenin and blocks the function of E-cadherin in cell adhesion, suggesting a role for phosphoregulation in maintaining this association [11]. Consistent with these data, *in vitro* phosphorylation of E-cadherin using multiple protein kinases enhances the binding of E-cadherin to β-catenin [11,21]. Measurements in solution using ITC suggest this enhancement is dramatic (>100-fold) [41]. However, it has remained unclear which sites within cadherin isoforms are actually subject to phosphorylation *in vivo*. Our data indicate that at least three sites within the β-catenin binding domain of cadherin are phosphorylated in *C. elegans* embryos. A key phosphorylated residue in HMR-1 is serine 1212, equivalent to serine 840 in human E-cadherin, which was suggested previously to be phosphorylated and contribute to β-catenin binding [11,33]. Thus, our data are consistent with previous work, but extend our understanding of the cadherin/β-catenin binding interface by identifying two additional, conserved phosphorylated residues that further contribute to this association. Moreover, our findings suggest that phosphorylation of these additional residues does not act cooperatively with serine 1212 phosphorylation in binding to β-catenin. Instead, they appear to further strengthen the association by acting in an additive manner. Notably, mutation of serines 847 (equivalent to serine 1218 identified in our study) and 840 to alanine was shown recently to alter and destabilize E-cadherin distribution in human cells [33], consistent with our work.

In contrast with the positive impact of cadherin phosphorylation in CCC assembly, phosphorylation of β-catenin appears to promote CCC disassembly. Previous work suggested that tyrosine 654 in human β-catenin is subject to phosphorylation and may perturb its binding to E-cadherin [12]. Subsequent findings further suggested that tyrosine

phosphorylation of CCC complexes following acetaldehyde treatment causes a redistribution of E-cadherin and β-catenin from the intercellular junctions [42]. Although we failed to identify phosphorylation on homologous tyrosine residues in our study, we found that other sites in HMP-2 are phosphorylated *in vivo* and affect HMP-2 binding to HMR-1 *in vitro*. Based on sequence alignments, we have been unable to demonstrate conservation of these phosphorylated residues in human β-catenin. Nevertheless, the function of the modification appears to be conserved, although our studies suggest that HMP-2 phosphorylation plays a relatively minor role as compared with HMR-1 phosphorylation in controlling HMP-2 distribution *in vivo*. It is also feasible that other proteins participate in regulating the association between HMR-1 and HMP-2 *in vivo*, which are not negatively affected by HMP-2 phosphorylation. The existence of such a factor would mask the impact of HMP-2 phosphorylation on its association with HMR-1 *in vivo*, but not *in vitro*, as we observed. Alternatively, phosphorylation ofHMP-2 may regulate adherens junctions in a manner that does not directly involve its association with HMR-1. Future studies that define the structure of the HMR-1/HMP-2 interface should be informative in understanding how phosphorylation of HMP-2 modulates its ability to associate with HMR-1.

Unlike mammalian αE-catenin, which forms homodimers in solution that bind well to actin *in vitro* [43], full-length *C. elegans* HMP-1 is a stable monomer and binds very weakly to actin, either alone or in complex with HMR-1 and HMP-2 [21]. The mechanism by which HMP-1 links CCCs to the underlying cytoskeleton has thus remained unclear. In isolation, the HMP-1 actin-binding domain is functional, suggesting that the full-length protein is auto-inhibited in solution [21]. Hence, we considered a potential role for HMP-1 phosphorylation in relieving its putative auto-inhibited state. To our surprise, phosphomimetic mutations in HMP-1 failed to substantially alter its global conformation in solution or affect its ability to bind actin. One reason for this could relate to our use of phosphomimetic substitutions, which may not create the appropriate chemical environment necessary to recapitulate that generated by phosphorylation [44]. However, the use of *in vitro* kinase reactions also have shortcomings and often lead to the modification of targets at non-specific sites, which would confound the interpretation of any resulting data from their use. Alternatively, a more modest, localized change in conformation may occur in response to phosphorylation, although the role for such an alteration remains unknown. Nonetheless, at least one residue in HMP-1 that we showed is phosphorylated *in vivo* (serine 649) is conserved in mammalian αE-catenin and has been identified as being phosphorylated in multiple global proteomic analyses in a variety of human cell lines (see http://www.phosphosite.org). Thus, a functional role for α-catenin phosphorylation may be conserved through evolution, and recent findings highlight its potential importance for strong cell–cell adhesion *in vivo* [45].

ACKNOWLEDGEMENTS

We thank S. Butcher for helpful discussions, the Advanced Photon Source staff for technical support, and members of the Audhya lab for critically reading this manuscript.

FUNDING

This work was supported by the American Heart Association [grant number SDG3720032 (to A.A.)]; the National Institutes of Health [grant numbers GM088151, GM110567 (to A.A.), MH067880, GM103533 (to J.R.Y.),

GM058038, HD072769 (to J.H.), RR02781, RR08438 and S100RR027000 (to S.E.B.), P41RR02301, P41GM66326 and P41GM10399]; and the National Science Foundation [grant numbers DMB-8415048, OIA-9977486 and BIR-9214394].

Abbreviations

CCC	cadherin–catenin complex
CK1	casein kinase I
DOGS-NTA-Ni	1,2-dioleoyl-sn-glycero-3-[(*N*-(5-amino-1-carboxypentyl) iminodiacetic acid) succinyl] nickel salt
MudPIT	multidimensional protein identification technology
PE	phosphatidylethanolamine
SEC–MALS	size-exclusion chromatography–multi-angle light scattering

REFERENCES

1. McEwen AE, Escobar DE, Gottardi CJ. Signaling from the adherens junction. Subcell. Biochem. 2012; 60:171–196. [PubMed: 22674072]
2. Leckband DE, de Rooij J. Cadherin adhesion and mechanotransduction. Annu. Rev. Cell Dev. Biol. 2014; 30:291–315. [PubMed: 25062360]
3. Takeichi M. Dynamic contacts: rearranging adherens junctions to drive epithelial remodelling. Nat. Rev. Mol. Cell Biol. 2014; 15:397–410. [PubMed: 24824068]
4. Bazzoni G, Dejana E. Endothelial cell-to-cell junctions: molecular organization and role in vascular homeostasis. Physiol. Rev. 2004; 84:869–901. [PubMed: 15269339]
5. Miller PW, Clarke DN, Weis WI, Nelson WJ. The evolutionary origin of epithelial cell-cell adhesion mechanisms. Curr. Top. Membr. 2013; 72:267–311. [PubMed: 24210433]
6. Giannotta M, Trani M, Dejana E. VE-cadherin and endothelial adherens junctions: active guardians of vascular integrity. Dev. Cell. 2013; 26:441–454. [PubMed: 24044891]
7. Oas RG, Nanes BA, Esimai CC, Vincent PA, Garcia AJ, Kowalczyk AP. p120-catenin and β-catenin differentially regulate cadherin adhesive function. Mol. Biol. Cell. 2013; 24:704–714. [PubMed: 23325790]
8. Ishiyama N, Ikura M. The three-dimensional structure of the cadherin-catenin complex. Subcell. Biochem. 2012; 60:39–62. [PubMed: 22674067]
9. Orsenigo F, Giampietro C, Ferrari A, Corada M, Galaup A, Sigismund S, Ristagno G, Maddaluno L, Koh GY, Franco D, et al. Phosphorylation of VE-cadherin is modulated by haemodynamic forces and contributes to the regulation of vascular permeability *in vivo*. Nat. Commun. 2012; 3:1208. [PubMed: 23169049]
10. Fujita Y, Krause G, Schefner M, Zechner D, Leddy HE, Behrens J, Sommer T, Birchmeier W. Hakai, a c-Cbl-like protein, ubiquitinates and induces endocytosis of the E-cadherin complex. Nat. Cell Biol. 2002; 4:222–231. [PubMed: 11836526]
11. Lickert H, Bauer A, Kemler R, Stappert J. Casein kinase II phosphorylation of E-cadherin increases E-cadherin/beta-catenin interaction and strengthens cell-cell adhesion. J. Biol. Chem. 2000; 275:5090–5095. [PubMed: 10671552]
12. Roura S, Miravet S, Piedra J, Garcia de Herreros A, Dunach M. Regulation of E-cadherin/catenin association by tyrosine phosphorylation. J. Biol. Chem. 1999; 274:36734–36740. [PubMed: 10593980]
13. Aberle H, Schwartz H, Kemler R. Cadherin-catenin complex: protein interactions and their implications for cadherin function. J. Cell Biochem. 1996; 61:514–523. [PubMed: 8806074]

14. Brady-Kalnay SM, Rimm DL, Tonks NK. Receptor protein tyrosine phosphatase PTPmu associates with cadherins and catenins *in vivo*. J. Cell Biol. 1995; 130:977–986. [PubMed: 7642713]
15. Behrens J, Vakaet L, Friis R, Winterhager E, Van Roy F, Mareel MM, Birchmeier W. Loss of epithelial differentiation and gain of invasiveness correlates with tyrosine phosphorylation of the E-cadherin/beta-catenin complex in cells transformed with a temperature-sensitive v-SRC gene. J. Cell Biol. 1993; 120:757–766. [PubMed: 8425900]
16. d'Azzo A, Bongiovanni A, Nastasi T. E3 ubiquitin ligases as regulators of membrane protein trafficking and degradation. Traffic. 2005; 6:429–441. [PubMed: 15882441]
17. Nanes BA, Kowalczyk AP. Adherens junction turnover: regulating adhesion through cadherin endocytosis, degradation, and recycling. Subcell. Biochem. 2012; 60:197–222. [PubMed: 22674073]
18. Hardin J, Lynch A, Loveless T, Pettitt J. Cadherins and their partners in the nematode worm *Caenorhabditis elegans*. Prog. Mol. Biol. Transl. Sci. 2013; 116:239–262. [PubMed: 23481198]
19. Achilleos A, Wehman AM, Nance J. PAR-3 mediates the initial clustering and apical localization of junction and polarity proteins during *C. elegans* intestinal epithelial cell polarization. Development. 2010; 137:1833–1842. [PubMed: 20431121]
20. Legouis R, Gansmuller A, Sookhareea S, Bosher JM, Baillie DL, Labouesse M. LET-413 is a basolateral protein required for the assembly of adherens junctions in *Caenorhabditis elegans*. Nat. Cell Biol. 2000; 2:415–422. [PubMed: 10878806]
21. Kwiatkowski AV, Maiden SL, Pokutta S, Choi HJ, Benjamin JM, Lynch AM, Nelson WJ, Weis WI, Hardin J. *In vitro* and *in vivo* reconstitution of the cadherin-catenin-actin complex from *Caenorhabditis elegans*. Proc. Natl. Acad. Sci. U.S.A. 2010; 107:14591–14596. [PubMed: 20689042]
22. Audhya A, Hyndman F, McLeod IX, Maddox AS, Yates JR, Desai A, Oegema K. A complex containing the Sm protein CAR-1 and the RNA helicase CGH-1 is required for embryonic cytokinesis in Caenorhabditis elegans. J. Cell Biol. 2005; 171:267–279. [PubMed: 16247027]
23. Cheeseman IM, Niessen S, Anderson S, Hyndman F, Yates JR, Oegema K, Desai A. A conserved protein network controls assembly of the outer kinetochore and its ability to sustain tension. Genes Dev. 2004; 18:2255–2268. [PubMed: 15371340]
24. Xu T, Venable JD, Park S, Cociorva D, Lu B, Liao L, Wohlschlegel J, Hewel J, Yates JR. ProLuCID, a fast and sensitive tandem mass spectra-based protein identification program. Mol. Cell Proteomics. 2006; 5:S174.
25. Dephoure N, Gould KL, Gygi SP, Kellogg DR. Mapping and analysis of phosphorylation sites: a quick guide for cell biologists. Mol. Biol. Cell. 2013; 24:535–542. [PubMed: 23447708]
26. Beausoleil SA, Villen J, Gerber SA, Rush J, Gygi SP. A probability-based approach for high-throughput protein phosphorylation analysis and site localization. Nat. Biotech. 2006; 24:1285–1292.
27. Wyatt PJ. Light-scattering and the absolute characterization of macromolecules. Anal. Chim. Acta. 1993; 272:1–40.
28. Konarev PV, Volkov VV, Sokolova AV, Koch MHJ, Svergun DI. PRIMUS: a Windows PC-based system for small-angle scattering data analysis. J. Appl. Cryst. 2003; 36:1277–1282.
29. Putnam CD, Hammel M, Hura GL, Tainer JA. X-ray solution scattering (SAXS) combined with crystallography and computation: defining accurate macromolecular structures, conformations and assemblies in solution. Q. Rev. Biophys. 2007; 40:191–285. [PubMed: 18078545]
30. Fyfe I, Schuh AL, Edwardson JM, Audhya A. Association of the endosomal sorting complex ESCRT-II with the Vps20 subunit of ESCRT-III generates a curvature-sensitive complex capable of nucleating ESCRT-III filaments. J. Biol. Chem. 2011; 286:34262–34270. [PubMed: 21835927]
31. Zaidel-Bar R, Joyce MJ, Lynch AM, Witte K, Audhya A, Hardin J. The F-BAR domain of SRGP-1 facilitates cell-cell adhesion during *C. elegans* morphogenesis. J. Cell Biol. 2010; 191:761–769. [PubMed: 21059849]
32. Lynch AM, Grana T, Cox-Paulson E, Couthier A, Cameron M, Chin-Sang I, Pettitt J, Hardin J. A genome-wide functional screen shows MAGI-1 is an L1CAM-dependent stabilizer of apical junctions in *C. elegans*. Curr. Biol. 2012; 22:1891–1899. [PubMed: 22981773]

33. McEwen AE, Maher MT, Mo R, Gottardi CJ. E-cadherin phosphorylation occurs during its biosynthesis to promote its cell surface stability and adhesion. Mol. Biol. Cell. 2014; 25:2365–2374. [PubMed: 24966173]
34. Stappert J, Kemler R. A short core region of E-cadherin is essential for catenin binding and is highly phosphorylated. Cell Adhes. Commun. 1994; 2:319–327. [PubMed: 7820535]
35. Choi H, Loveless T, Lynch AM, Bang I, Hardin J, Weis W. A conserved phosphorylation switch controls the interaction between cadherin and β-catenin *in vitro* and *in vivo*. Dev. Cell. 2015; 33:82–93. [PubMed: 25850673]
36. Korswagen HC, Herman MA, Clevers HC. Distinct beta-catenins mediate adhesion and signaling functions in *C. elegans*. Nature. 2000; 406:527–532. [PubMed: 10952315]
37. Maiden SL, Harrison N, Keegan J, Cain B, Lynch AM, Pettitt J, Hardin J. Specific conserved C-terminal amino acids of *Caenorhabditis elegans* HMP-1/α-Catenin modulate F-actin binding independently of vinculin. J. Biol. Chem. 2013; 288:5694–5706. [PubMed: 23271732]
38. Tande BM, Wagner NJ. Viscosimetric, hydrodynamic, and conformational properties of dendrimers and dendrons. Macromolecules. 2001; 34:8580–8585.
39. Hoschuetzky H, Aberle H, Kemler R. Beta-catenin mediates the interaction of the cadherin-catenin complex with epidermal growth factor receptor. J. Cell. Biol. 1994; 127:1375–1380. [PubMed: 7962096]
40. Liu D, el-Hariry I, Karayiannakis AJ, Wilding J, Chinery R, Kmiot W, McCrea PD, Gullick WJ, Pignatelli M. Phosphorylation of beta-catenin and epidermal growth factor receptor by intestinal trefoil factor. Lab. Invest. 1997; 77:557–563. [PubMed: 9426392]
41. Choi HJ, Huber AH, Weis WI. Thermodynamics of beta-catenin-ligand interactions: the roles of the N- and C-terminal tails in modulating binding affinity. J. Biol. Chem. 2006; 281:1027–1038. [PubMed: 16293619]
42. Sheth P, Seth A, Atkinson KJ, Ghey T, Kale G, Giorgianni F, Desiderio DM, Li C, Naren A, Rao R. Acetaldehyde dissociates the PTP1B–E-cadherin–b-catenin complex in Caco-2 cell monolayers by a phosphorylation-dependent mechanism. Biochem. J. 2007; 402:291–300. [PubMed: 17087658]
43. Drees F, Pokutta S, Yamada S, Nelson WJ, Weis WI. Alpha-catenin is a molecular switch that binds E-cadherin–beta-catenin and regulates actin-filament assembly. Cell. 2005; 123:903–915. [PubMed: 16325583]
44. Hunter T. Why nature chose phosphate to modify proteins. Phil. Trans. R. Soc. Lond. B. Biol. Sci. 2012; 367:2513–2516. [PubMed: 22889903]
45. Escobar DJ, Desai R, Ishiyama N, Folmsbee SS, Novak MN, Flozak AS, Daugherty RL, Mo R, Nanavati D, Sarpal R, et al. α-Catenin phosphorylation promotes intercellular adhesion through a dual-kinase mechanism. J. Cell Sci. 2015; 128:1150–1165. [PubMed: 25653389]

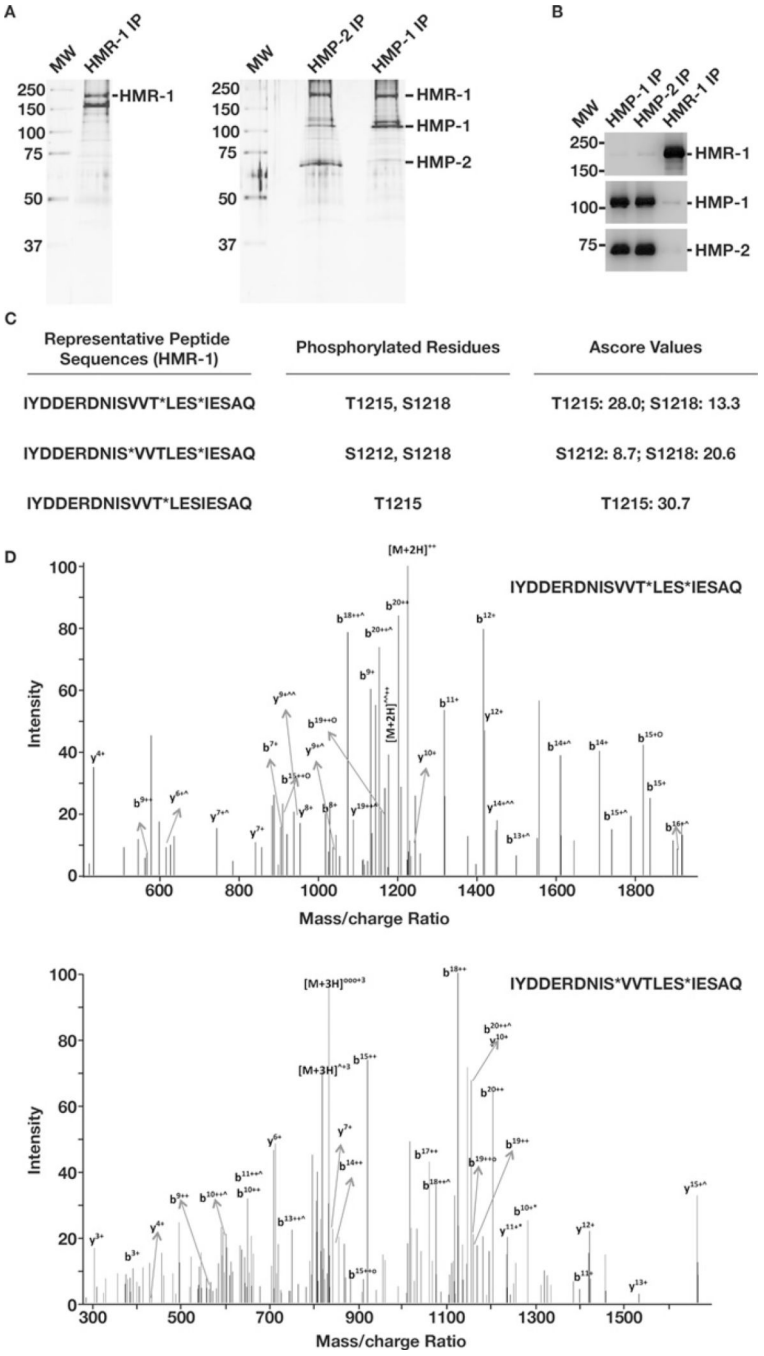

Figure 1. HMR-1 is phosphorylated *in vivo*

(**A**) SDS/PAGE analysis of HMR-1, HMP-1 and HMP-2 immunoprecipitations following silver staining. A molecular weight marker (MW) is shown (left), and the likely positions of HMR-1, HMP-1 and HMP-2 are indicated (right) for each gel. The length of time to silver stain the gel showing the HMR-1 immunoprecipitation (left) was substantially longer than that taken for the other gel (right). (**B**) Immunoblot analysis of HMR-1, HMP-1 and HMP-2 immunoprecipitates using antibodies directed against each protein is shown. (**C**) Representative peptides uncovered during phosphoproteomic analysis of a HMR-1

immunoprecipitate. Phosphorylated residues in each peptide are highlighted by asterisks, and their Ascore values are shown (right). Residues with Ascore values >19 have >99% accuracy, whereas values >3 have >80% accuracy (23). (**D**) Representative, hand-annotated MS/MS spectra for two analysed HMR-1 peptides are shown. The symbols o, * and îndicate the neutral losses of H_2O, NH_3 and H_4PO_3, respectively.

A

Representative Peptide Sequences (HMP-1)	Phosphorylated Site	Ascore Values
IVSGSAS*IADAESTR	S312	24.8
LLTTALDNITTLDDFLAVS*EAHIVEDCER	S509	23.1
SMNDVDS*DVEYEADGVGAANADANR	S649	40.2
NEIETGRDS*DDEELDR	S910	44.4

B

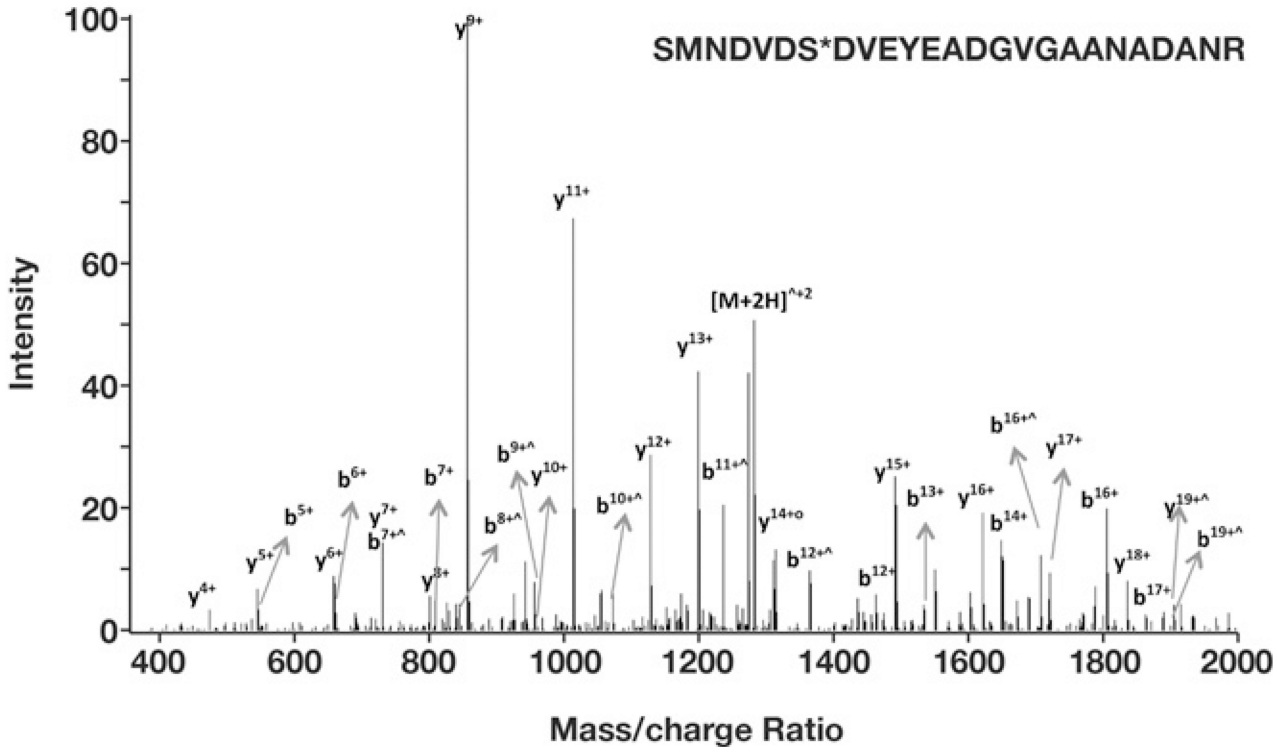

Figure 2. HMP-1 is phosphorylated *in vivo*

(**A**) Representative peptides uncovered during phosphoproteomic analysis of a HMP-1 immunoprecipitate. Phosphorylated residues in each peptide are highlighted by asterisks, and their Ascore values are shown (right). (**B**) Representative, hand-annotated MS/MS spectrum for an analysed HMP-1 peptide is shown. The symbols o, * and îndicate the neutral losses of H_2O, NH_3 and H_4PO_3, respectively.

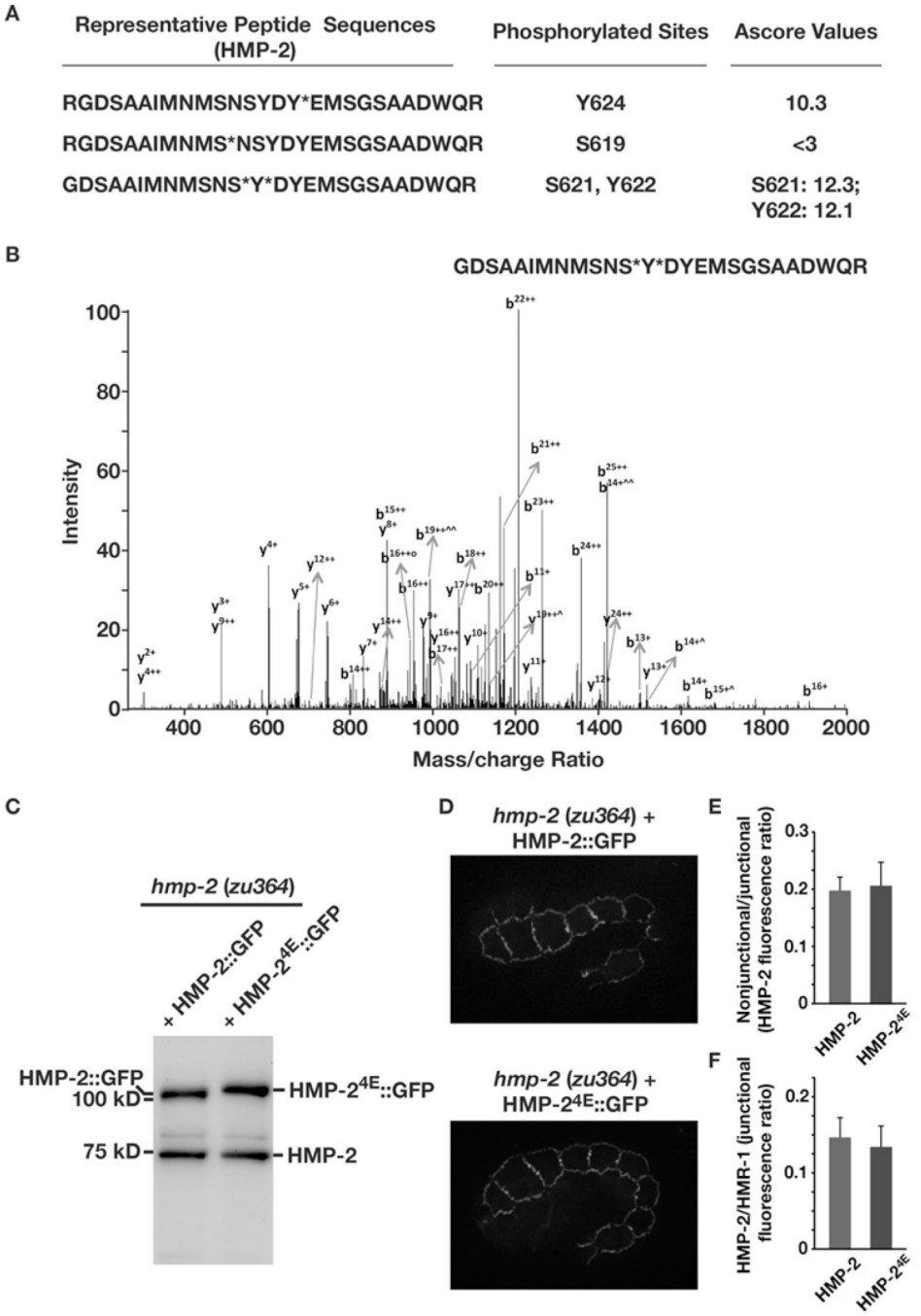

Figure 3. HMP-2 is phosphorylated *in vivo*

(**A**) Representative peptides uncovered during phosphoproteomic analysis of a HMP-2 immunoprecipitate. Phosphorylated residues in each peptide are highlighted by asterisks, and their Ascore values are shown (right). (**B**) A representative, hand-annotated MS/MS spectrum for an analysed HMP-2 peptide is shown. The symbols o, * and îndicate the neutral losses of H_2O, NH_3 and H_4PO_3, respectively. (**C**) Homozygous *hmp-2* (*zu364*) mutant animals expressing either wild-type HMP-2::GFP or HMP-2^{4E}::GFP were lysed in sample buffer, and the equivalent of 10 animals were separated by SDS/PAGE in each case.

Immunoblot analysis using HMP-2 antibodies was conducted to determine the relative expression of the transgenes as compared with endogenous HMP-2. Based on densitometry measurements, the GFP fusion proteins are each expressed at ~1.3-fold the level of the endogenous (non-functional) HMP-2. (**D**) Homozygous *hmp-2* (*zu364*) mutant embryos expressing HMP-2::GFP or HMP-2^{4E}::GFP were imaged using confocal fluorescence (GFP) microscopy. Scale bar, 10 μm. (**E** and **F**) Animals expressing HMP-2::GFP or HMP-2^{4E}::GFP in the *hmp-2* (*zu364*) mutant background were fixed and stained using antibodies directed against HMR-1. The amount of nonjunctional and junctional HMP-2 in each case was calculated based on intensity measurements (**E**), and a ratio of HMP-2 and HMR-1 fluorescence at junctions was also determined (**F**). Data shown are based on more than 10 embryos examined for each transgenic strain. Error bars represent the mean ± S.E.M. No statistically significant difference was found following *t*-test analysis in either case.

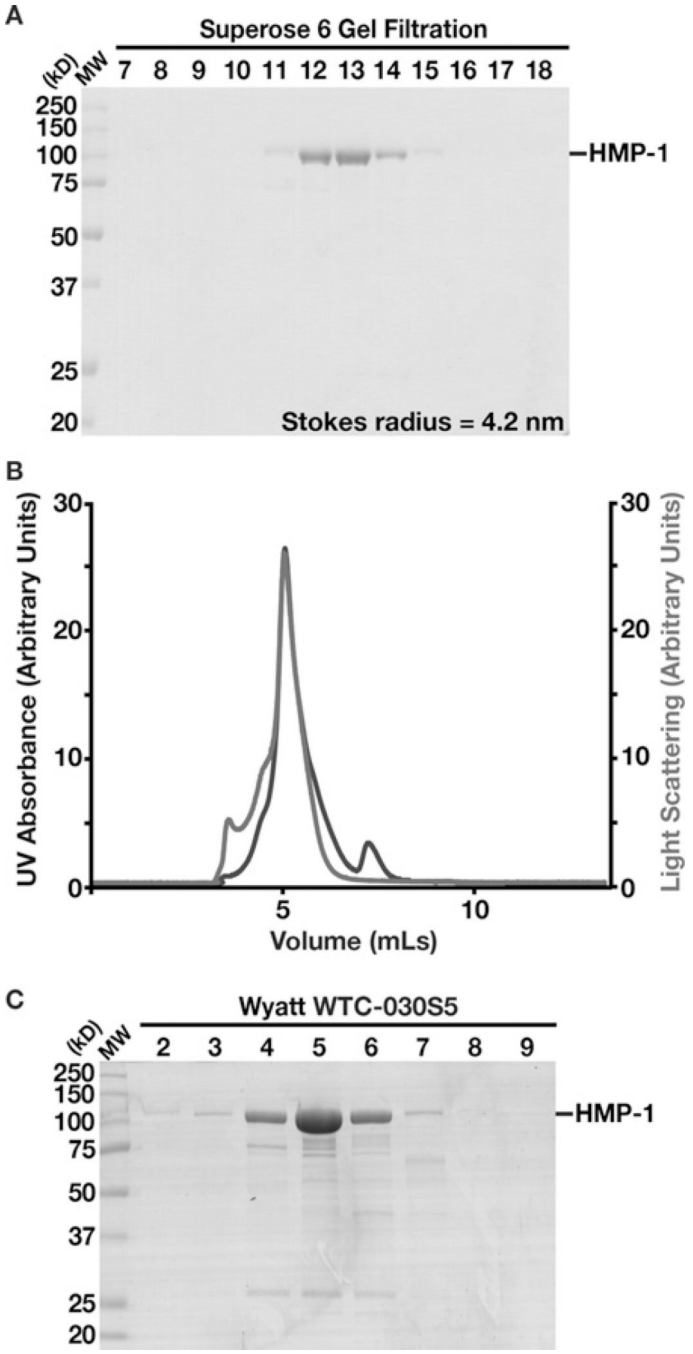

Figure 4. Recombinant HMP-1 is a stable monomer in solution

(**A**) Purified, recombinant HMP-1 was separated over a Superose 6 gel filtration column, and its Stokes radius was calculated based on the elution profiles of known standards. The data shown are representative of at least three independent experiments. (**B** and **C**) Recombinant HMP-1 was separated over a Wyatt WTC-030S5 gel filtration column that was coupled to a multi-angle light-scattering device. Both the UV absorbance (dark line) and light-scattering (light line) profiles are plotted (middle) and eluted fractions were

separated by SDS/PAGE and stained using Coomassie to highlight the elution profile of HMP-1 (bottom).

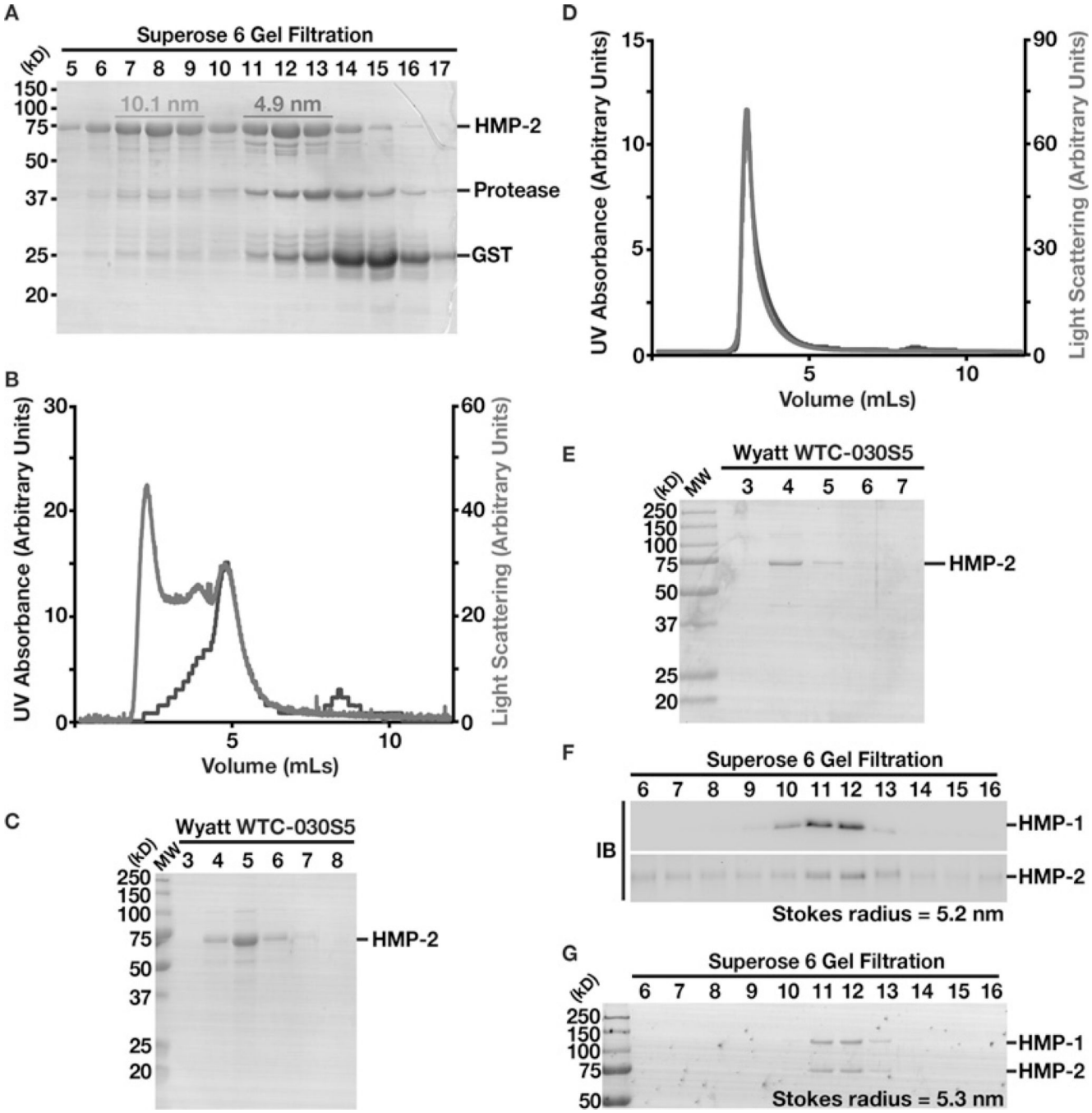

Figure 5. Recombinant HMP-2 self-associates in the absence of HMP-1

(**A**) Recombinant HMP-2 was purified as a GST fusion protein, subject to Prescission protease cleavage in solution to remove the GST tag, and separated over a Superose 6 gel filtration column. The Stokes radii of two HMP-2 populations were calculated based on the elution profiles of known standards (highlighted). The data shown are representative of at least three independent experiments. (**B–E**) Each pool of recombinant HMP-2 (fractions 7–9 in panel **D** and fractions 11–13 in panel **B**) was separated over a Wyatt WTC-030S5 gel filtration column that was coupled to a multi-angle light-scattering device. Both the UV

absorbance (dark line) and light-scattering (light line) profiles are plotted (**B** and **D**) and eluted fractions were separated by SDS/PAGE and stained using Coomassie to highlight the elution profiles of each HMP-2 population (**C** and **E**). Astra software was used to calculate the molecular mass of HMP-2 in each population. (**F**) Wild-type *C. elegans* embryo extract was separated over a Superose 6 gel filtration column, and fractions were separated by SDS/PAGE for immunoblot analysis using HMP-1 (top) or HMP-2 (bottom) antibodies. (**G**) Recombinant HMP-1 and HMP-2 were co-expressed, purified and separated over a Superose 6 gel filtration column. The Stokes radius of the HMP-1/HMP-2 complex was calculated based on the elution profiles of known standards. The data shown are representative of at least three independent experiments.

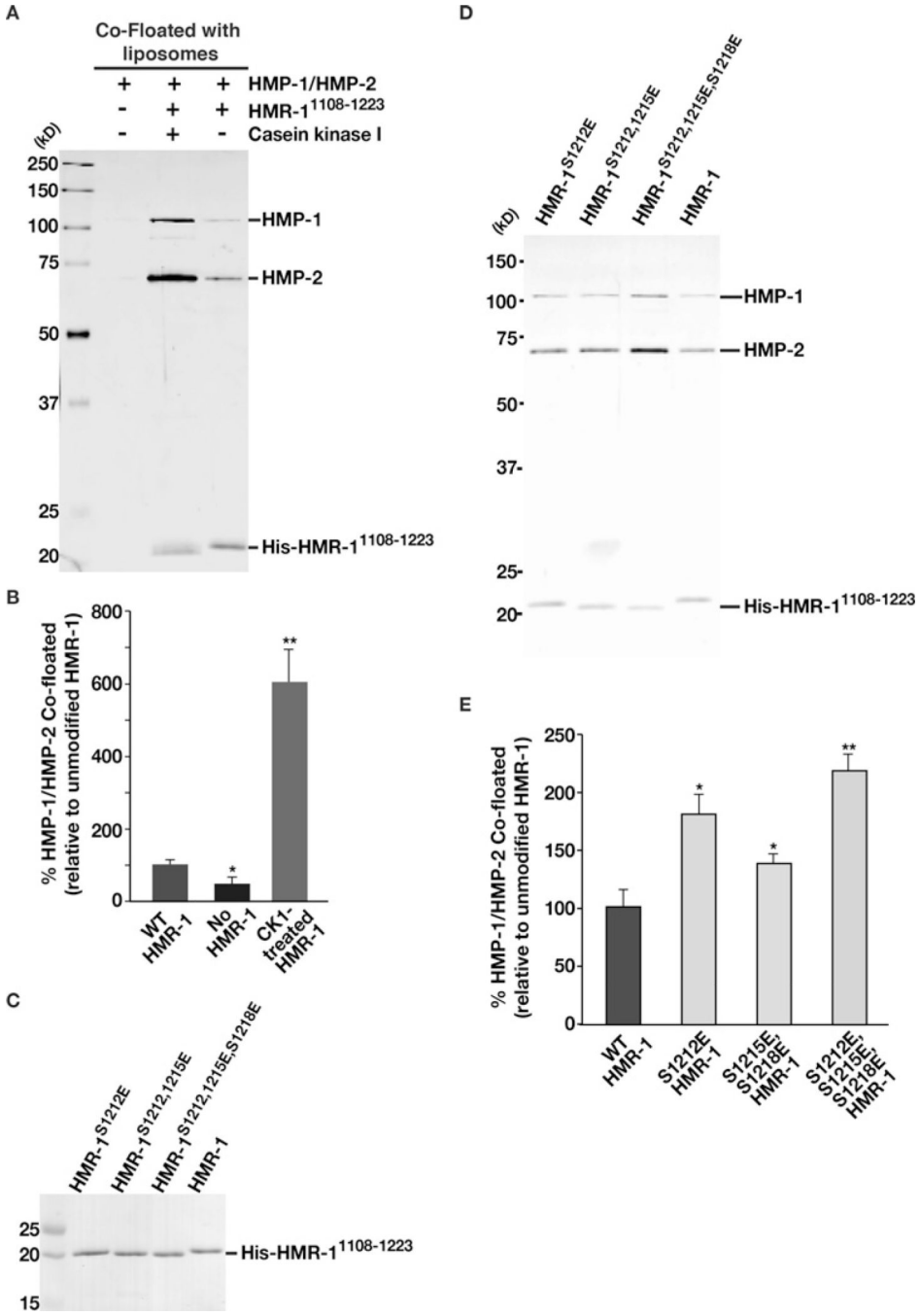

Figure 6. Phosphomimetic mutations in HMR-1 enhance its ability to bind HMP-1/HMP-2 complexes on lipid bilayers

(**A** and **D**) Purified HMP-1/HMP-2 complexes were co-incubated with DOGS-NTA-Ni-containing liposomes in the presence or absence of various poly-histidine tagged forms of HMR-1$^{1108–1223}$ and floated through an Accudenz gradient. Co-floated proteins were recovered at the top of the gradient, normalized based on liposome concentration, separated by SDS/PAGE, and silver-stained. Data shown are representative of more than three experiments conducted independently. (**B** and **E**) Quantification of the percentages of

HMP-1/HMP-2 recovered after co-flotation experiments performed in panels A ($n = 3$) and D ($n = 6$). Error bars represent the mean ± S.E.M. (*, $P < 0.05$; **, $P < 0.01$; *t*-test). (**C**) Various forms of recombinant HMR-$1^{1108–1223}$ were separated by SDS/PAGE and stained using Coomassie.

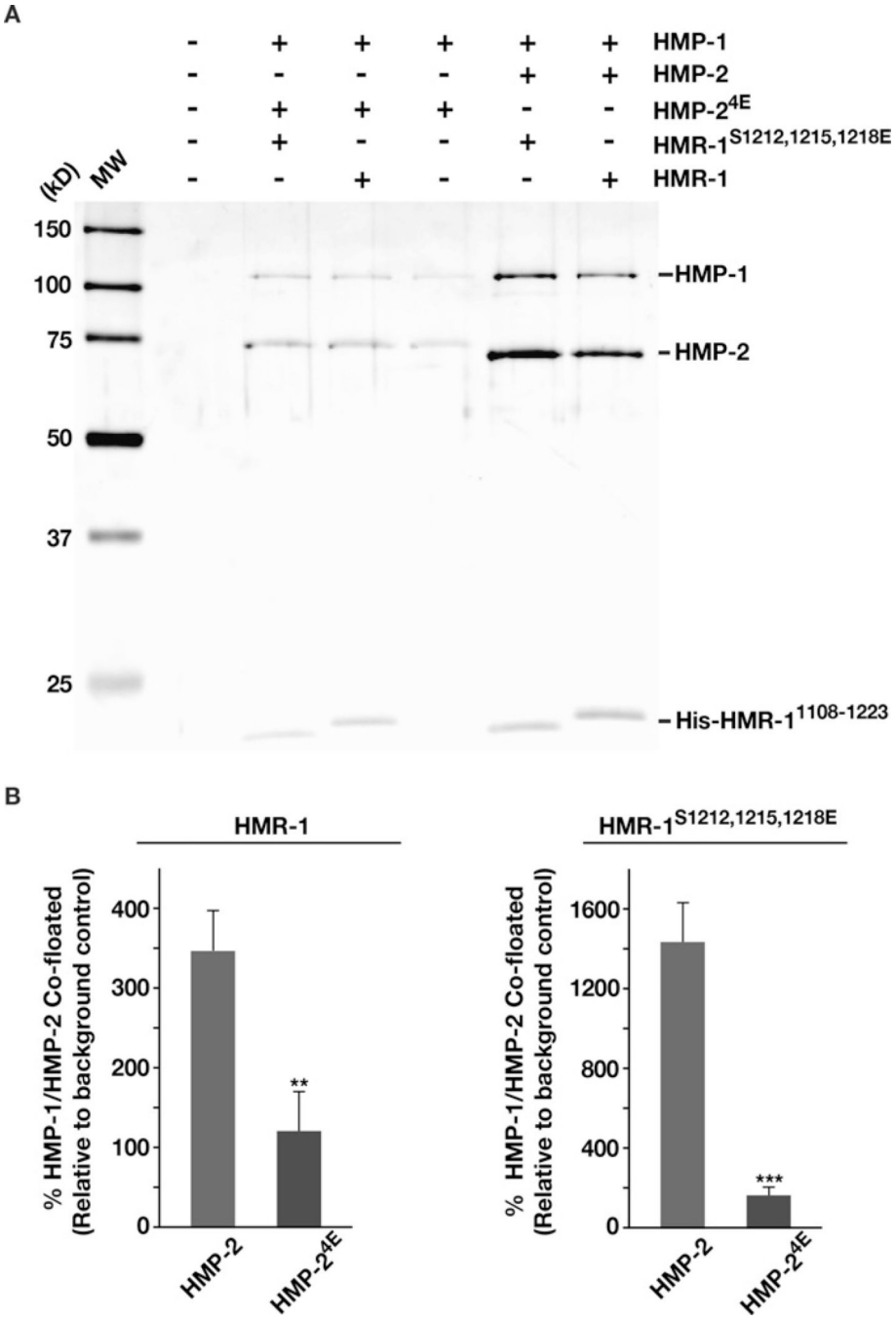

Figure 7. Phosphomimetic mutations in HMP-2 impair its association with HMR-1

(**A**) Purified HMP-1/HMP-2 complexes (containing either wild-type or phosphomimetic HMP-2) were co-incubated with DOGS-NTA-Ni-containing liposomes in the presence or absence of various poly-histidine tagged forms of HMR-1$^{1108–1223}$ and floated through an Accudenz gradient. Co-floated proteins were recovered at the top of the gradient, normalized based on liposome concentration, separated by SDS/PAGE, and silver-stained. Data shown are representative of more the four experiments conducted independently. (**B**) Quantification of the percentages of HMP-1/HMP-2 recovered after co-flotation

experiments performed in panel A ($n = 4$). Error bars represent the mean ± S.E.M. (**, $P < 0.01$; ***, $P < 0.001$; *t*-test).

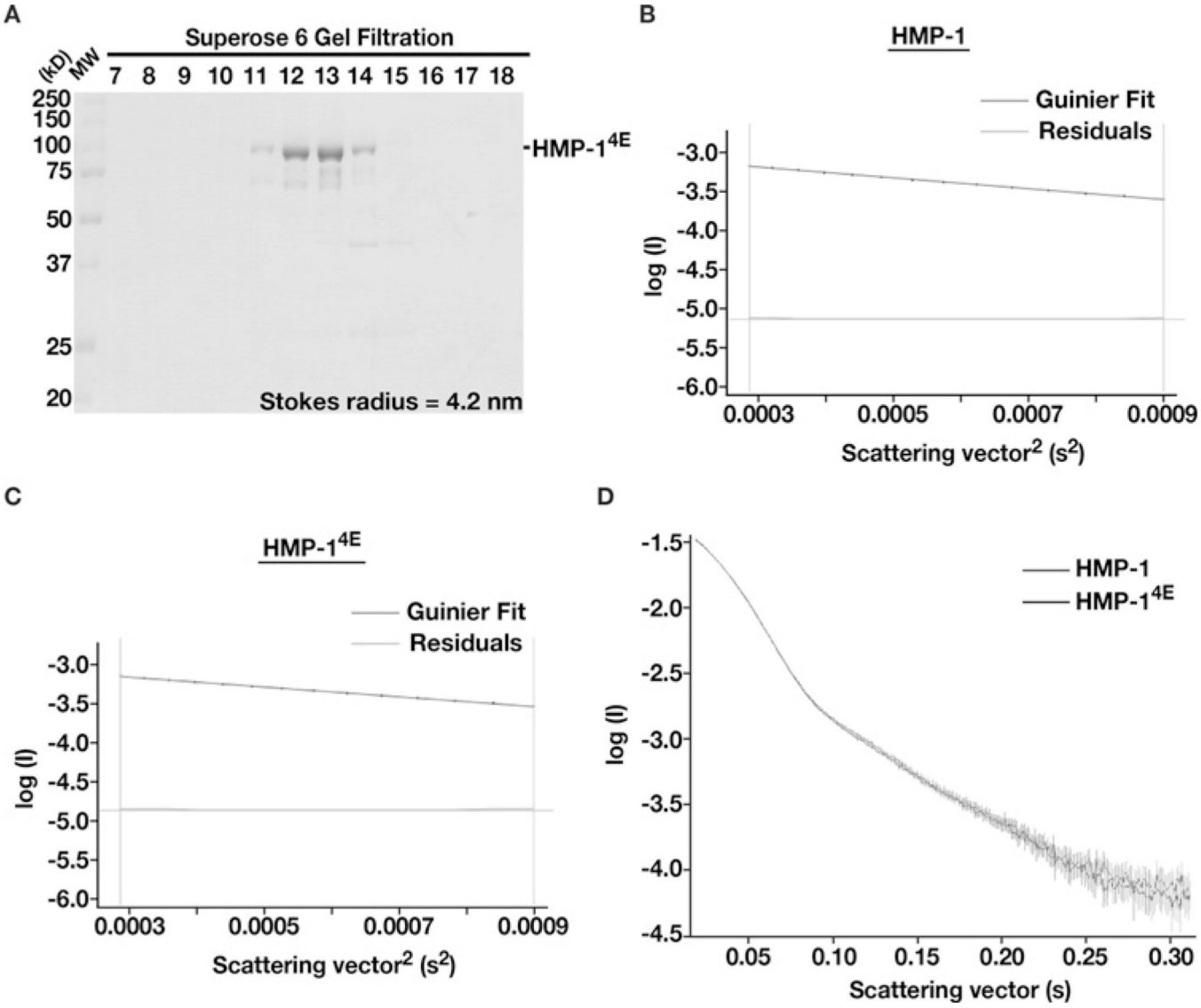

Figure 8. Phosphomimetic mutations in HMP-1 do not affect its global conformation in solution

(**A**) Purified, recombinant HMP-1^{4E} was separated over a Superose 6 gel filtration column, and its Stokes radius was calculated based on the elution profiles of known standards. The data shown are representative of at least three independent experiments. (**B** and **C**) Wild-type and phosphomimetic HMP-1 were analysed by SAXS, and the resulting Guinier plots are shown. The lack of curvature in the residuals plots suggests linear behaviour for both proteins. Data shown are representative of multiple SAXS studies. (**D**) An overlay of the scattering vectors for wild-type HMP-1 and HMP-1^{4E}, as a function of the log of the SAXS intensities, reveals highly similar profiles for both proteins.

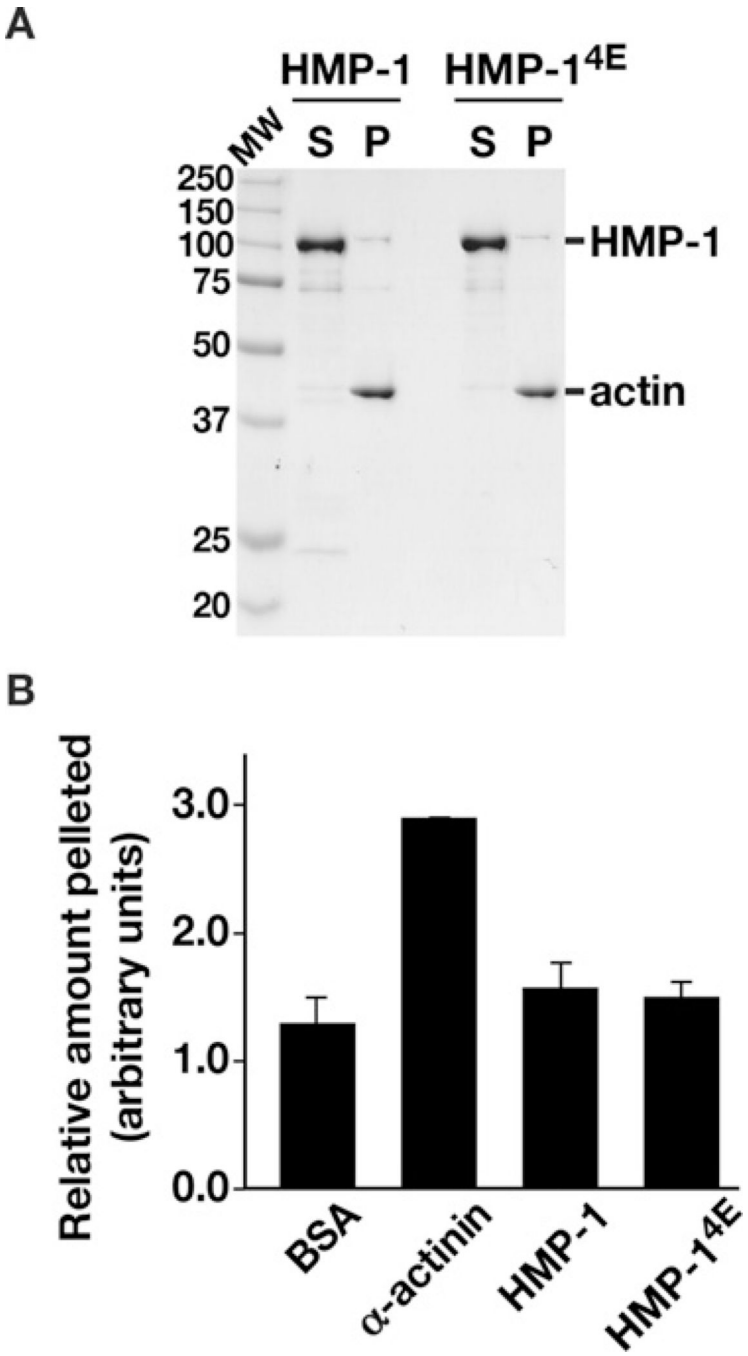

Figure 9. Phosphomimetic mutations in HMP-1 do not affect its inability to bind to actin

(**A**) Actin pelleting assays using BSA (negative control), α-actinin (positive control), and wild-type and phosphomimetic forms of recombinant HMP-1 were conducted with varying concentrations of actin (2 μM shown). Proteins co-pelleting with actin (P) or in the supernatant (S) subsequent to centrifugation were recovered, separated by SDS/PAGE, and stained using Coomassie. (**B**) Quantification of the relative amount of protein co-pelleting

with actin (2 and 5 μM), normalized for the amount of actin recovered. Error bars represent the mean ± S.E.M. (n = 4).

Table 1

Identification of HMR-1, HMP-1, and HMP-2 interacting partners using immunoprecipitation (IP) followed by solution mass spectrometry

		% Sequence coverage			
***C. elegans* gene**	**Human homologue(s)**	**HMR-1 (IP)**	**HMP-1 (IP)**	**HMP-2 (IP)**	**Predicted size (kDa)**
hmr-1 (W02B9.1)	E-cadherin	57.6	28.6	5.5	133.5
hmp-1 (R13H4.4)	αE-catenin	19.0	77.2	61.4	104.0
hmp-2 (K05C4.6)	β-catenin	15.8	53.4	49.6	74.5
jac-1 (Y105C5B.21)	p120 catenin	5.7	5.9	5.4	138.3
afd-1 (W03F11.6)	afadin	3.7	12.7	3.3	183.6
srgp-1 (F12F6.5)	srGAP1	–	7.5	2.1	120.2
magi-1 (K01A6.2)	MAGI1	–	4.9	37.2	115.2

Table 2

Results from gel filtration analysis of HMP-1/HMP-2 complexes harbouring different phosphomimetic mutations

Complex	Average stokes radius (n = 3)
HMP-1/HMP-2	5.3 nm
HMP-1^{4E}/HMP-2	5.2 nm
HMP-1/HMP-2^{4E}	5.3 nm
HMP-1^{4E}/HMP-2^{4E}	5.3 nm

Table 3

Radius of gyration as determined using SAXS for wild-type and phosphomimetic HMP-1

Protein	Average radius of gyration (Å)
HMP-1 (1 mg/ml)	41.1 ± 1.2
HMP-1 (2.5 mg/ml)	41.6 ± 0.8
HMP-1 (5 mg/ml)	42.2 ± 0.5
HMP-1^{4E} (1 mg/ml)	41.9 ± 1.2
HMP-1^{4E} (2.5 mg/ml)	42.6 ± 0.6
HMP-1^{4E} (5 mg/ml)	43.0 ± 0.6